

A Novel Smart High-Voltage Circuit Breaker for Smart Grid Applications

Jun Liu, *Student Member, IEEE*, Garng M. Huang, *Senior Member, IEEE*, Zhiying Ma, *Senior Member, IEEE*, and Yingsan Geng, *Senior Member, IEEE*

Abstract—In this paper, we propose a new “intelligent operation” concept for high-voltage SF₆ gas circuit breakers, in which the moving contacts are self-adaptively controlled from one position to an adjacent position to improve the circuit breaker life cycles. To analyze the concept intelligent operation, a new model of high-voltage SF₆ gas circuit breaker is developed, and the moving characteristics of the new type circuit breaker are computed based on the newly designed model. Then both mechanical and electrical wears are quantitatively analyzed according to the breaker’s new moving characteristic. Finally, we demonstrate the life cycle improvement of the new type of high-voltage SF₆ gas circuit breaker. Our analysis can also be used to estimate the remaining life cycle of a breaker based on the tallied data collected by our intelligent modules.

Index Terms—Electrical wear, high-voltage SF₆ gas circuit breaker, intelligent operation, mechanical wear, phase control technology, reliability.

I. INTRODUCTION

CIRCUIT breakers have been playing a critical electrical apparatus role to control and protect power equipments including power transmission lines for high-voltage power systems during faults. It has become even more essential for smart grid applications even during normal operations: the smart grid needs to break or make rated current more frequently besides the function of fault protection. For examples, optimal transmission switching is able to cut the generation costs greatly based on optimal power flow analysis [1]. It is also shown that branch and bus coupler switching [2] is a powerful control option to find optimum robust network topologies. In addition, [3] shows that network reconfiguration can alleviate or remove the potential overload of a monitored line. In addition to transmission switching, researches on the important role of interruptible loads [4], [5] in deregulated electricity markets to ensure both power system security and optimum electricity prices also have been

demonstrated; hence, circuit breakers will be required to perform more normal operations (i.e., load shedding) under rated current in the distribution network of future smart grid. To meet the demands for these smart grid applications, it is pertinent to develop new technology to lengthen life cycles (the number of operations) of high-voltage breakers for transmission systems for more reliable operations.

Ever since SF₆ gas was discovered in the 1900s, the development of high-voltage circuit breakers has made considerable progress. Nowadays, SF₆ gas circuit breakers (GCBs) have become the mainstream of the high-voltage market, and have been widely used in all applications involving power system voltages in the range of 72.5 kV to 800 kV [6]. Although SF₆ has greenhouse effect, it is exclusively used as an insulation and quenching medium for high-voltage circuit breakers because of its high insulation strength and high interruption capability of fault current at present; while alternative medium, such as vacuum, limits its use only to voltages up to 100 kV [7]. Our objective here is to enhance breaker reliability by lengthening its lifetime in such a way that the breaker will need less maintenance and serve longer time in power systems. The implication is that less SF₆ need to be produced and used for GCBs, which will induce considerable environmental benefits.

Historically, the development of high-voltage SF₆ GCB has experienced three periods, namely, the two-pressure [8] stage, the puffer type stage, and the hybrid type circuit breaker stage. A hybrid type GCB has the mixed structure of self-blast thermal expansion type and puffer type GCB. A novel GCB named intelligent circuit breaker is proposed in this paper. Conventionally, circuit breaker is considered unintelligent on its own. Former researches of circuit breakers focused mainly on monitoring the SF₆ gas parameters [9], the control circuit status [10] of GCB, etc. Traditional GCB receives an open-or-close signal from relays, and then operates simply according to its factory setting, which cannot be modified or adjusted for different situations. To increase life cycles, we propose to develop intelligent controls on the operating mechanism to improve the basic interrupting characteristic of GCBs to meet the demands of smart grid applications for GCBs’ critical role for frequent rated current operations. The proposed intelligent operation of high-voltage gas circuit breakers take advantage of the advancement of digital circuits and flexible hydraulic valve regulators to lengthen the operation life cycles of breakers with relatively low extra cost. Our data and analysis confirm the effectiveness of our approach: the life cycles of both faulted and normal operations can be increased substantially since our intelligent control unit will reduce both electrical and mechanical wears substantially. Our analysis can also be used to predict the remaining lifetime of

Manuscript received January 12, 2010; revised June 09, 2010, September 30, 2010, December 08, 2010; accepted January 29, 2011. Date of current version May 25, 2011. This work was supported in part by the China Scholarship Council and Texas A&M University, College Station. Paper no. TSG-00005-2010.

J. Liu, Z. Ma, and Y. Geng are with State Key Laboratory of Electrical Insulation and Power Equipments, Department of Electrical Engineering, Xi’an Jiaotong University, Xi’an, Shaanxi 710049, China (e-mail: jliu1912@gmail.com; zyma@mail.xjtu.edu.cn; ysgeng@mail.xjtu.edu.cn).

G. M. Huang is with Department of Electrical and Computer Engineering, Texas A&M University, College Station, TX 77843-3128 USA (e-mail: ghuang@tamu.edu).

Color versions of one or more of the figures in this paper are available online at <http://ieeexplore.ieee.org>.

Digital Object Identifier 10.1109/TSG.2011.2134113

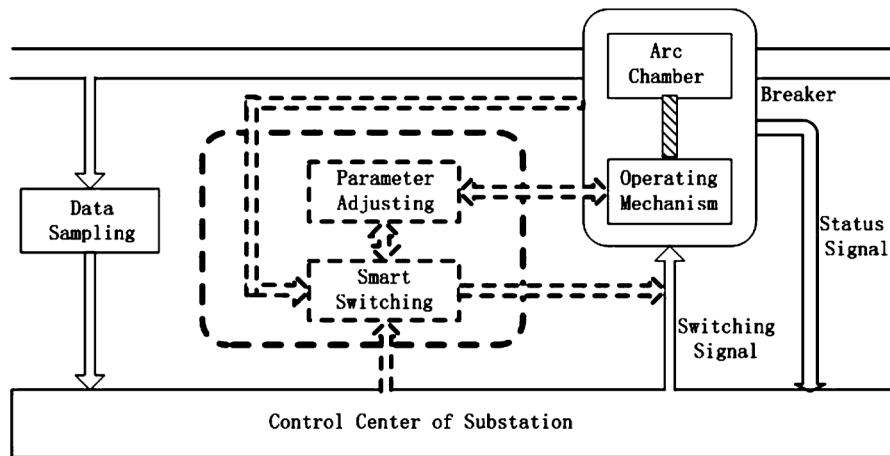


Fig. 1. Principal block diagram of intelligent operation of circuit breakers.

GCBs using the manufacturer's empirical data of the breakers through our smart control modules. The remaining life cycle estimate can also serve as a vital input to the future just-in-time maintenance scheduling of intelligent GCBs.

II. PRINCIPLES OF INTELLIGENT OPERATION OF SF₆ GAS CIRCUIT BREAKERS

So far, gas circuit breakers can only operate with a fixed moving characteristic as designed, despite of various system conditions. However, it is obvious that the switching requirements of GCBs are rather different under different power system operation conditions, such as no load, normal load, and short-circuit faults. In fact, an ideal opening characteristic, determined by the gap size, contact moving speed, etc., should vary according to system conditions. When GCB opens short-circuit faults, it has to overcome high energy electric arc; in contrast, it has low arcing burden while opening during normal load situations. Traditionally, circuit breakers are designed to have only one opening characteristic, which is independent of breaking current values. As a consequence, the characteristic is designed for the worst scenario that the contact system has to move at a high speed to reduce the electrical wear; thus it shortens the life cycle since it renders unnecessary stress on the mechanical components of GCBs.

In high-voltage GCB terminology, *Operation* is defined as "conversion of the moving contact from one position to another," according to IEC standard [11]. Here a new concept of an *Intelligent Operation* is proposed as an "adaptive conversion of the moving contact from one position to another." GCB with intelligent operation can automatically adjust its operating mechanism, based on the power system real-time data. Accordingly, the new type of circuit breakers will have more opening characteristics; for example, it will open a no-load circuit at a lower speed to reduce its mechanical wear, but break a fault circuit at a much higher speed to reduce its electrical wear. In this way, GCBs will have longer life cycle and need less maintenance.

The proposed intelligent operation GCB (IOGCB) consists of a conventional circuit breaker structure and an additional intelligent control unit (ICU) introduces some new functions to the equipment. As a result, the novel IOGCB, whose block diagram

is introduced in Fig. 1, will require no changes to the present structure of substations and relay protection systems.

As shown in Fig. 1, the blocks with solid lines denote the components in a conventional GCB and its connections to transmission lines and substation remains the same. The dashed line block denotes the intelligent control unit (ICU) that is added to the circuit breaker for the function of intelligent operation. The ICU is composed of two modules: Smart Switching Module and Parameter Adjusting module.

1) Smart Switching Module is the core part of the ICU, which is a microprocessor controller system.

The microprocessor controller has four basic functions. First function is to receive real-time current magnitude and phase angle values from protection relays, which is sent before the open/close decision so that the adjusting device can have enough time to change its parameters. It also sends the status signal of the breaker to the relay and control center.

The second function is to perform an online operation that selects an operation mode and associated characteristic setting values for the parameter adjusting module based on the relay current magnitude data and predesigned thresholds. In practice, the thresholds are decided and setting values are saved from those precomputed characteristic modes designed offline based on field data.

The third function is to acquire both mechanism status information and tally each operation for overall statistics for maintenance purposes.

Its final function is to send the trip-or-close signal to the breaker control coil to initiate the operation at an appropriate phase that can reduce the arc magnitude and duration after it receives the final trip-or-close signal from the relay.

2) Parameter Adjusting Module changes the parameters of the operating mechanism to the setting values selected from the second function so that it can operate at different speeds according to power system conditions. This is a desirable module that is applicable to all generic breakers. In this paper we propose an adjusting regulating device that consists of a high-speed controllable hydraulic valve, which can be easily switched to different modes according to the signal from the intelligent microprocessor for our puffer type GCBs. The adjusting device should adjust its parameters during the relay coordination time.

We limit our presentation on the basics of the parameter adjusting module and second function of the smart switching due to space limitation. We also introduce the rudimentary for the third statistic function to show the effectiveness our novel approach. The last function is to trip at an optimal switching phase, which will be addressed also.

The ICU which includes a microprocessor system (cost in hundreds or so), a high-speed regulating valve (costs in tens or so) and the cost of software development, which is a small percentage compared to tens of thousands dollars of a high-voltage CB. And the microprocessor system can be reliable if it satisfies electromagnetic compatibility, as many digital relay microprocessors have successfully demonstrated [12].

The added high-speed regulating valve to control the interrupting characteristics may slightly introduce some more complexity to the original mechanical operating mechanism. However, the extra ICU can reduce the failure rate on mechanical components of breakers through continuous monitoring, including linkages, latches, energy storage system, compressor, actuator, damper, valves, etc., which represent about 44% of total breaker failures during the CIGRE second international enquiry on high-voltage circuit breaker reliability [13]. The inspection and maintenance tasks on the extra valve are needed regularly by electric power utilities as part of the regular mechanical component maintenance procedure.

III. MODIFYING MOVING CHARACTERISTICS OF SF₆ PUFFER TYPE CIRCUIT BREAKERS THROUGH A REGULATING VALVE

Most high-voltage SF₆ circuit breakers' arc-quenching chambers are made in a puffer type, operated by hydraulic or pneumatic operating mechanism. This paper takes the hydraulic operating mechanism as an example to illustrate our new concept. The following theoretical model is based on empirical data of the 126 kV SF₆ puffer type circuit breaker from China Pinggao Electric Corp. [14].

The two key parts in a GCB, namely the operating mechanism and arc-quenching chamber, always interact and influence each other. Operating mechanism drives the contact system to move in the chamber via a moving characteristic. The moving characteristic of a GCB is described by the opening velocity based on Newton's Second Law:

$$M_C \frac{dv}{dt} = F_y - F_p - F_b - F_f \quad (1)$$

where M_C denotes the equivalent mass of the moving contact system, v is the velocity of the moving contact, F_y is the operating force of the hydraulic mechanism, F_p is the counterforce by the compression cylinder in the arc extinguishing chamber, F_b is the buffering force, and F_f denotes the friction force. It is clear then that changing the above forces will change its moving characteristic. In this paper, we propose to change the moving characteristic by modifying F_y as follows.

From the working principle of hydraulic mechanism [15], [16], operating force of the hydraulic operating mechanism F_y can be expressed as

$$F_y = (P_f S_H - P_0 S_L) - \left(S_H \sum k_{1i}^2 \xi_{1i} + S_L \sum k_{2i}^2 \xi_{2i} \right) v^2 \quad (2)$$

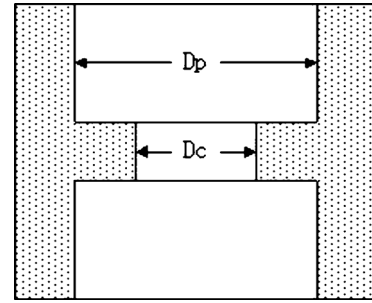


Fig. 2. Control of the oil pipeline diameter.

in which P_f is the gas pressure in pressure storage, ξ_{1i}, ξ_{2i} are pressure loss coefficients of high pressure oil pipeline corresponding to low-pressure oil pipeline in the hydraulic mechanism, k_{1i}, k_{2i} are ratios of the velocity of oil in the high pressure pipeline and low-pressure pipeline to the velocity of moving contact, S_H, S_L are true work areas of the piston's two sides, namely the side of high pressure oil and the side of low-pressure oil. Define the following terms to simplify (2) as follows:

$$\begin{aligned} F_0 &= (P_f S_H - P_0 S_L), \\ C_{PL} &= S_H \sum k_{1i}^2 \xi_{1i} + S_L \sum k_{2i}^2 \xi_{2i} \\ &= S_H \sum k_{1i}^2 \left(1 - \frac{D_c^2}{D_p^2} \right) + S_L \sum k_{2i}^2 \left(1 - \left(\frac{D_c^2}{D_p^2} \right) \right). \end{aligned} \quad (3)$$

Hence (2) is simplified as

$$F_y = F_0 - C_{PL} v^2. \quad (4)$$

From (4), it can be seen that F_y is composed of two parts F_0 and $C_{PL} v^2$. F_0 is preacting force, which is the static output force of operating hydraulic piston; and it relates to the structural parameters of hydraulic operating mechanism, interlocking pressure P_f inside pressure storage, and oil pressure P_0 inside auxiliary oil tank. When $P_f = 25.8$ MPa, F_0 is about 20 kN. C_{PL} is overall pipeline loss coefficient (in unit: N·s²/m²). It shows that the oil pressure overall loss is related to the hydraulic pipeline mechanism, effective piston area of cylinder and oil properties. D_c and D_p are the diameters of the controlled pipeline, as shown in Fig. 2.

The overall pipeline loss coefficient C_{PL} is selected as our controllable parameter. From [17], it is known that the oil flows through the pipeline to form pressure force to the piston, as shown in Fig. 2; normal hydraulic operating mechanism only has a fixed pipe diameter D_p .

In order to control the overall pipeline loss coefficient C_{PL} , high-speed hydraulic regulating valves are added to change the diameter of the original pipeline. From [18], it indicates that modern technology is able to lower the adjusting time of high-speed valves to less than 3 ms with a standard deviation of two percent; thus, the control system can make the additional adjusting time acceptable, or even negligible, by the power system interrupting constraints. When the oil runs through the aperture, the oil flow contracts first and then expands, because the controllable diameter of aperture D_c is smaller than that of the pipe D_p . Consequently, part of the oil pressure will be lost; so we

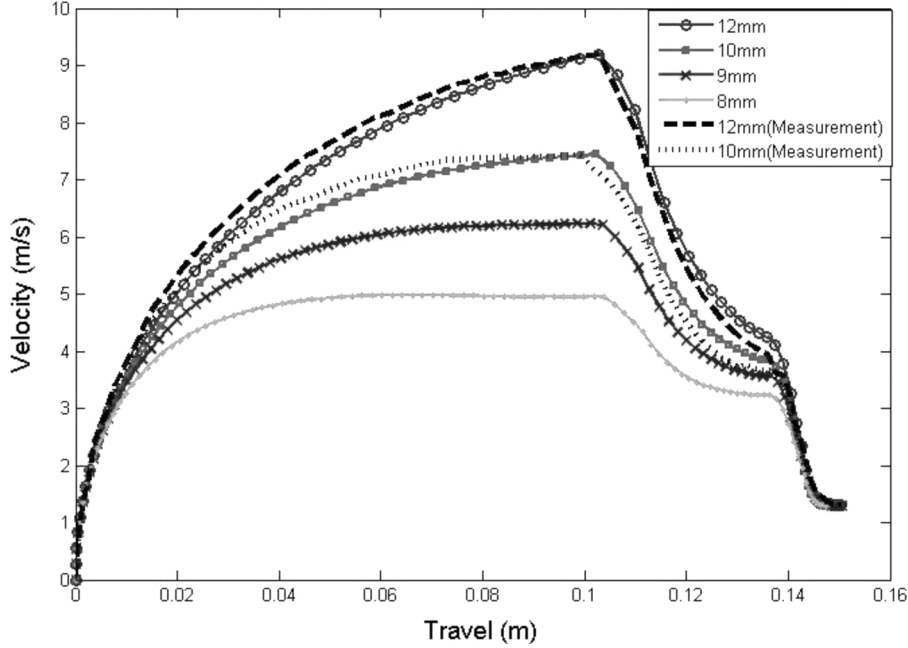


Fig. 3. Experimental and theoretical opening characteristics with different drain oil apertures.

can change the pipeline loss coefficient by controlling the parameter D_c through the regulating valve. From (4), it can be concluded that the velocity of GCB's operating mechanism will be adjustable simply by changing the coefficient C_{PL} ; some of our results about pipeline loss coefficients of GCB can be seen in [19]. As for the GCB presently in use, the adjustable opening characteristic is achieved by changing the diameter of the drain oil aperture. In our research, controllable regulating valves are adopted because it is quantitatively adjustable to control the coefficient C_{PL} in order to achieve intelligent operation for SF₆ GCBs.

Counterforce of the cylinder to the moving system F_p is decided by the shape, size of working area and the pressure difference between the inside and outside cylinder

$$F_p = \iint_S (p - p_0) d\vec{S} \cdot \vec{z}_0 \quad (5)$$

where p is gas pressure inside the cylinder; p_0 is gas pressure outside the cylinder; S is compressed surface; and \vec{z}_0 is unit vector of moving direction.

Equation (5) describes the action of the return force of the cylinder. When moving contact compresses the SF₆ gas inside the cylinder, the pressure increment will cause a reaction force to resist further compression. It is worth noting that the thermal energy of arc has also been taken into consideration in our model to change the value of gas pressure p . Here F_p is decided by the pressure difference between the inside and outside cylinder and the bearing area of the cylinder.

Buffer force F_b is a reaction force of the buffer at the end of breaker travel, which is designed to absorb high kinetic energy to decrease the big impact force so that parts of the mechanism will not be damaged. Buffer force is related to clearance width and contact velocity

$$F_b = \frac{3}{4} \frac{\pi \eta l_b D_b^3}{\delta^3} v \quad (6)$$

where δ is clearance width between the buffer contact and buffer cavity, l_b is buffer contact travel, η is dynamic viscosity of hydraulic oil [20]. Friction force F_f can be given by experiment or experience. Here in our research, we use 1000 N for our calculations. Plug all these forces into (1), the moving characteristic is determined.

After implementing the ICU to the selected 126 kV SF₆ puffer type circuit breaker from China Pinggao Electric Corp., our novel IOGCB is able to obtain the required minimum initial opening velocity successfully under different opening modes. For example, during a special short-circuit fault clearing case study, the minimum initial opening velocity of 7.0 m/s is achieved to break a 100% rated short-circuit current; compared to 4.5 m/s for the 10% rated short-circuit current. Moreover, our intelligent GCB model is able to break without load situation (thus no current) at any specified low speed.

The theoretical data matches the opening speed measurements on 126 kV SF₆ puffer type circuit breaker from China Pinggao Electric Corp. well. More calculation results are shown in Fig. 3 based on our new intelligent GCB model; the dashed and dotted curves are measurement velocity data from 3 kA rated current interruptions, compared to 12 mm and 10 mm calculated velocity curves from our theoretical model with “○” and “■” markers separately.

We have also made tests on our ICU circuit hardware and DSP multitask software system, the result of which satisfies the real-time requirement of intelligent operation. We use simulated short-circuit currents and rated symmetrical sinusoidal currents from EMTP software as input signal from instrumental transformers on site, to test the intelligent identification of different power system working status. Several current thresholds are set in our ICU to indicate different interrupting duties for our smart circuit breaker, and therefore mode control signals are sent to the regulating valve to obtain various opening speeds. And through both hardware and software testing procedures above, it has

been proven that the ICU is able to adjust high-speed regulating valves precisely according to the simulated power system current signals in our laboratory [21].

IV. WEAR AND LIFE CYCLE ANALYSIS

Both electrical and mechanical wear [22] contribute to contact material loss; and the lifetime of circuit breakers depends largely on the quality of the electrical contacts. Electrical wear relates to factors such as the form of the contacts, ac or dc switching, contact speed, and contact pressure. Mechanical wear relates to the nature of the material, the form of the contacts, their relative movement, and the pressure between them.

A. Influence of Contact Speed on Electrical Wear

Successful alternate current interruption depends on whether the dielectric withstanding capability of the SF₆ gap is greater than the increasing voltage that is being impressed across the gap by the circuit in an attempt to reestablish the flow of current [8].

The calculation of the dielectric strength is quite complicated. It relates to many factors, such as:

- 1) properties of the dielectric;
- 2) distance between contacts;
- 3) nonuniform coefficients of electric field;
- 4) surface roughness of the electrodes;
- 5) density of gas molecule.

Since our smart CB changes the opening speed to adapt to various power system conditions, we focus our wear analysis on its impacts by the moving contact travel, which is characterized by the contact speed and arcing time and assume that all other factors remain the same. Also, due to space limitation, we simplify our presentation by assuming that interruption will not fail after current-zero, which means that reigniting issue is avoided in our analysis. We also use phase control in our smart CB, we will also investigate the combining effects of contact speeds and phase control in terms of arcing time.

That is to say, after arcing time t_{arc} , the dielectric strength of SF₆ can withstand recovery voltage when the distance between contacts reaches a certain value L_{gap} . This value can be acquired by the integral of contact moving speed $v(t)$, and average speed is used to simplify our representation of integration

$$L_{gap} = \int_0^{t_{arc}} v(t) dt \triangleq v_{average} \cdot t_{arc}. \quad (7)$$

According to the theory of electrical contacts [23], the main contact electrical wear is contributed by electric arc energy. Electrical wear of contacts is

$$W_e = \int_0^{t_{arc}} K_w |i(t)/I_{scN}|^\beta dt \quad (8)$$

where K_w is a coefficient relating to arc-extinguishing medium, cooling condition, contact moving speed, and contact material, and β is decided by experiments, $1 < \beta \leq 3$, $i(t)$ denotes the real-time current value during an interruption, and I_{scN} denotes rated short-circuit breaking current value of the particular circuit breaker given by the manufacturer.

Based on (8), it can be easily concluded that contact electrical wear will be more serious if the breaking current is higher

and the arcing time is longer. To find the influence of contact speed on electrical wear, we use average speed, defined by (7), to simplify our presentation and the speed is acquired from the velocity curves from Fig. 3.

As an example, in 50 Hz electrical power system, whose fundamental cycle T_s is 20 ms; the nonintelligent SF₆ GCB (our original 126 kV SF₆ puffer type circuit breaker model) can break a certain short-circuit current when the SF₆ dielectric strength reaches $L_{gap} = 24$ mm. If the average speed of moving contact is $v_0 = 4.8$ m/s, the shortest arcing time permitted will be 5 ms, which means the optimum arc duration is one quarter cycle (namely 90°). During the lifetime of a GCB, the open or close signal from protective relays may occur at any phase angle randomly, hence the actual arcing time t_{arc} varies with arc starting phase angle θ . As seen in Fig. 4, because the least arcing time is one quarter cycle, the angle difference between the next zero crossing point (180°, 360°, 540°...) and arc starting angle should be greater than 90° so as to reach enough dielectric strength. The arcing time duration will be a segmented function of arc starting angle when no fault currents are present

$$t'_{arc} = \begin{cases} t'_1 = \frac{180^\circ - \theta}{360^\circ} * T_s \text{ (ms)} & (0^\circ < \theta \leq 90^\circ) \\ t'_2 = \frac{360^\circ - \theta}{360^\circ} * T_s \text{ (ms)} & (90^\circ < \theta \leq 180^\circ) \\ t'_3 = \frac{360^\circ - \theta}{360^\circ} * T_s \text{ (ms)} & (180^\circ < \theta \leq 270^\circ) \\ t'_4 = \frac{540^\circ - \theta}{360^\circ} * T_s \text{ (ms)} & (270^\circ < \theta \leq 360^\circ). \end{cases} \quad (9)$$

Statistically, arc starting angle will occur randomly from 0° to 360°, so the average arcing time is $0.5T_s$ (average arc duration is 180°), it is much larger than our control objective 5 ms of circuit breakers with intelligent operation; and it can be calculated by

$$\overline{t'_{arc}} = \frac{180^\circ}{360^\circ} T_s = 0.5T_s = 10 \text{ ms}. \quad (10)$$

1) *Electrical Wear Analysis for Rated Current Operation With Both Phase Selection and Speed Control:* Synchronous switching [24] without varying contact speed has been researched over twenty years, since it is not easy to select the precise breaking phase angle. Our intelligent operation uses real-time voltage and current data for the microprocessor to find the optimal switching time for our IOGCB that can have varying contact speeds. When the smart GCB receives the open command for normal rated operations, with the phase control technology, the breaker will trip after a delay to ensure dielectric strength when current passes zero with an optimum arcing time to lessen the electrical wear; and the shortened arcing time without varying speed will be

$$t''_{arc} = \begin{cases} t''_1 = \frac{90^\circ}{360^\circ} * T_s \text{ (ms)} (0^\circ < \theta \leq 90^\circ, \text{ delay } 90^\circ - \theta) \\ t''_2 = \frac{90^\circ}{360^\circ} * T_s \text{ (ms)} (90^\circ < \theta \leq 180^\circ, \text{ delay } 270^\circ - \theta) \\ t''_3 = \frac{90^\circ}{360^\circ} * T_s \text{ (ms)} (180^\circ < \theta \leq 270^\circ, \text{ delay } 270^\circ - \theta) \\ t''_4 = \frac{90^\circ}{360^\circ} * T_s \text{ (ms)} (270^\circ < \theta \leq 360^\circ, \text{ delay } 360^\circ - \theta) \end{cases} \quad (11)$$

$$\overline{t''_{arc}} = \frac{90^\circ}{360^\circ} T_s = 0.5 \overline{t'_{arc}} = 0.25T_s. \quad (12)$$

Denote the contacts electrical wear as W_{e0} for an average contact speed of $v_0 = 4.8$ m/s of a conventional GCB. Consider

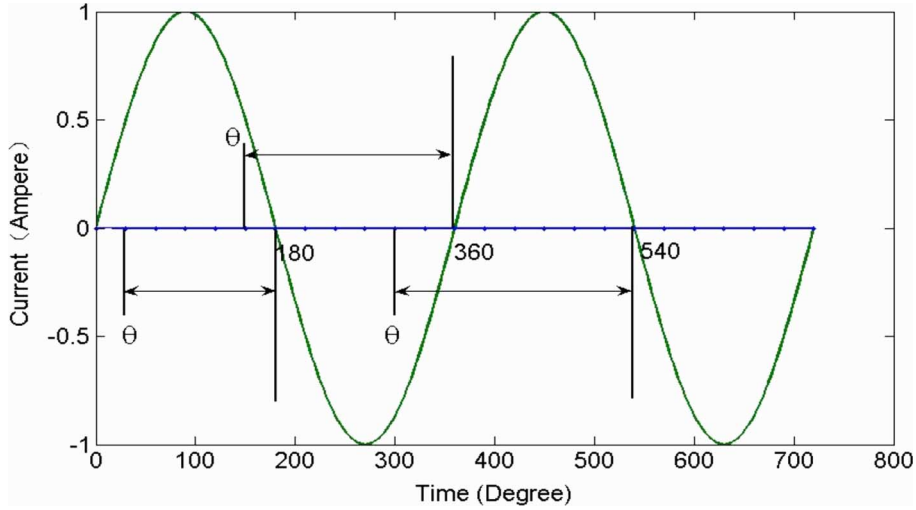


Fig. 4. Arcing time at different arc starting phase angle.

 TABLE I
 ELECTRICAL WEAR WITH DIFFERENT CONTACT SPEED ($T_s = 20$ ms)

	GCB w/o IO	Intelligent Operation GCB			
D_c (mm)	12	8	9	10	12
$v_{average}$ (m/s)	4.8	3.6	3.9	4.3	4.8
t_{arc} (w/o phase control)	t_{arc}	$1.333t_{arc}$	$1.228t_{arc}$	$1.116t_{arc}$	t_{arc}
t_{arc} (with- phase control)	$0.5T_s$	$0.333T_s$	$0.307T_s$	$0.279T_s$	$0.25T_s$
W_e	W_{e0}	$0.667W_{e0}$	$0.614W_{e0}$	$0.558W_{e0}$	$0.5W_{e0}$

our new intelligent GCB that the contact moving speed can be modified as needed: when the diameter of drain oil aperture D_c changes from 8 mm to 10 mm, the average speed of moving contact will change from $v_0 = 4.8$ m/s to a range from 3.6 m/s to 4.8 m/s, then average arcing time will be longer. After applying phase control technology, the average arcing time becomes

$$\overline{t_{arc}} = L_{gap}/v = v_0 \overline{t_{arc}''}/v = 0.25T_s v_0/v. \quad (13)$$

By adjusting the drain oil aperture D_c without phase technology the electric wear will increase; however, with the phase control technology, we further lessen the electrical wear. Table I shows that contacts electrical wear decreases as the contact speed decreases when phase technology is used.

From Table I, when the GCB break a rated current, it can operate at a lower opening speed by adjusting the pipeline diameter values, and then the average arcing time will decrease (i.e., the arcing time is $0.375T_s$ at the speed 3.6 m/s, compared to $0.5T_s$ at its original speed 4.8 m/s). For a rated current like 3 kA, when opening at 3.6 m/s, the contacts will only have 75% of the electrical wear with the speed of 4.8 m/s.

 TABLE II
 SIMPLE CALCULATION PARAMETERS

I_{dm} (kA)	T_d (s)	I_{am} (kA)	f (Hz)	θ (rad)
28.28	0.040	28.28	50	0

2) *Electrical Wear Analysis for Fault Current Operation:* For short-circuit fault operations, IOGCBs still need to open at the fastest speed so as to reach the required dielectric strength as soon as possible. The short-circuit current includes both dc decaying component and ac sinusoidal component, which implies that the average arcing time cannot be calculated by (9) and (11), since the current zero points will no longer occur at ($0^\circ, 180^\circ, 360^\circ, 540^\circ \dots$). A typical short-circuit fault current waveform is not symmetrical due to the dc decay, the waveform will have the so-called major loop and minor loop. To calculate the exact arcing time, we need to find the zero crossing points on the current waveform.

A typical short-circuit current always includes two parts, the dc decay component and ac sinusoidal component

$$i(t) = I_{dm} * e^{-t/T_d} + I_{am} * \sin(2\pi f * t + \theta) \quad (14)$$

where I_{dm} , I_{am} are the magnitude of dc and ac component, T_d is the dc the decaying time constant, f is the current frequency, and θ is the initial phase angle of the ac component. The parameters in (14) can be acquired through fast real-time algorithms [25] as shown in our previous research; here a set of values are chosen in Table II for arcing time analysis. The value of the fault current is 40 kA.

The smart circuit breaker should choose the fastest velocity to break the short-circuit fault current, which is at an average speed of 4.8 m/s with $D_c = 12$ mm. Since the SF₆ dielectric gap should be wider so as to force the arc to extinguish at the zero crossing point, the required gap parameter will be larger than rated current tripping. Here we choose an optimum gap as $L_{gap} = 24$ mm, then the optimum arcing time will be

$$t_{arc}^{min} = 0.005s = 5 \text{ ms}. \quad (15)$$

TABLE III
CURRENT ZERO CROSSING TIME IN MS FOR EXAMPLE GIVEN IN TABLE II

t_1	t_2	t_3	t_4	t_5	t_6	t_7	t_8	t_9	t_{10}
12.6	17.8	31.5	38.8	50.9	59.3	70.5	79.6	90.3	99.7

From the basic parameters in Table II, we can get the zero crossing time of this short-circuit fault in Table III.

Based on the results in Table III, the average arcing time of the fault at different tripping signal time t (in unit: millisecond) will be:

1) $0 \leq t < t_1 - 5$ ($0 \leq t < 7.6$)

$$\overline{t'_{\text{arc}1}} = t_{\text{arc}}^{\min} + \frac{(t_1 - t_{\text{arc}}^{\min}) - (0)}{2} \\ = 5 + 3.8 = 8.8$$

;

2) $t_1 - 5 \leq t < t_2 - 5$ ($7.6 \leq t < 12.8$)

$$\overline{t'_{\text{arc}2}} = t_{\text{arc}}^{\min} + \frac{(t_2 - t_{\text{arc}}^{\min}) - (t_1 - t_{\text{arc}}^{\min})}{2} \\ = t_{\text{arc}}^{\min} + \frac{t_2 - t_1}{2} = 5 + 2.6 = 7.6$$

;

3) $t_2 - 5 \leq t < t_3 - 5$ ($12.8 \leq t < 26.5$)

$$\overline{t'_{\text{arc}3}} = t_{\text{arc}}^{\min} + \frac{(t_3 - t_{\text{arc}}^{\min}) - (t_2 - t_{\text{arc}}^{\min})}{2} \\ = t_{\text{arc}}^{\min} + \frac{t_3 - t_2}{2} = 5 + 6.85 = 11.85$$

;

4) $t_3 - 5 \leq t < t_4 - 5$ ($26.5 \leq t < 33.8$)

$$\overline{t'_{\text{arc}4}} = t_{\text{arc}}^{\min} + \frac{(t_4 - t_{\text{arc}}^{\min}) - (t_3 - t_{\text{arc}}^{\min})}{2} \\ = t_{\text{arc}}^{\min} + \frac{t_4 - t_3}{2} = 5 + 3.65 = 8.65$$

;

5) $t_4 - 5 \leq t < t_5 - 5$ ($33.8 \leq t < 45.9$)

$$\overline{t'_{\text{arc}5}} = t_{\text{arc}}^{\min} + \frac{(t_5 - t_{\text{arc}}^{\min}) - (t_4 - t_{\text{arc}}^{\min})}{2} \\ = t_{\text{arc}}^{\min} + \frac{t_5 - t_4}{2} = 5 + 6.05 = 11.05$$

Notice that we limit our calculation to two ac cycles (that is about 40 ms in 50 Hz power system), because circuit breakers have to clear the short-circuit fault in two or three cycles so as not to damage power equipments and endanger the system reliability. Since the actual fault current waveform is no longer symmetrical, the distribution of $t'_{\text{arc}1}$ to $t'_{\text{arc}5}$ will be different depending on their intervals. The average arcing time will be

$$\overline{t'_{\text{arc}}} = \sum_{i=1}^5 w_i * \overline{t'_{\text{arc}i}} \\ = w_1 * \overline{t'_{\text{arc}1}} + w_2 * \overline{t'_{\text{arc}2}} + w_3 * \overline{t'_{\text{arc}3}} \\ + w_4 * \overline{t'_{\text{arc}4}} + w_5 * \overline{t'_{\text{arc}5}} \quad (16)$$

where the w_1 to w_5 denotes the probability of the arcing time occurring at those five intervals, and their summation should equal to one. In a total sample time of two cycles (one cycle $T = 20$ ms), the five weight parameters can be calculated as

$$w_1 = \frac{(t_1 - t_{\text{arc}}^{\min}) - (0)}{2T} = \frac{7.6 - 0}{40} = 0.19$$

$$w_2 = \frac{(t_2 - t_{\text{arc}}^{\min}) - (t_1 - t_{\text{arc}}^{\min})}{2T} \\ = \frac{t_2 - t_1}{2T} = \frac{12.8 - 7.6}{40} = 0.13$$

$$w_3 = \frac{(t_3 - t_{\text{arc}}^{\min}) - (t_2 - t_{\text{arc}}^{\min})}{2T} \\ = \frac{t_3 - t_2}{2T} = \frac{26.5 - 12.8}{40} = 0.3425$$

$$w_4 = \frac{(t_4 - t_{\text{arc}}^{\min}) - (t_3 - t_{\text{arc}}^{\min})}{2T} \\ = \frac{t_4 - t_3}{2T} = \frac{33.8 - 26.5}{40} = 0.1825$$

$$w_5 = \frac{2T - (t_4 - t_{\text{arc}}^{\min})}{2T} = \frac{40 - 33.8}{40} = 0.155.$$

So the average arcing time of the example is

$$\overline{t'_{\text{arc}}} = \sum_{i=1}^5 w_i * \overline{t'_{\text{arc}i}} \\ = \frac{(t_1 - t_{\text{arc}}^{\min}) - (0)}{2T} * \left(t_{\text{arc}}^{\min} + \frac{(t_1 - t_{\text{arc}}^{\min}) - (0)}{2} \right) \\ + \frac{t_2 - t_1}{2T} * \left(t_{\text{arc}}^{\min} + \frac{t_2 - t_1}{2} \right) \\ + \frac{t_3 - t_2}{2T} * \left(t_{\text{arc}}^{\min} + \frac{t_3 - t_2}{2} \right) \\ + \frac{t_4 - t_3}{2T} * \left(t_{\text{arc}}^{\min} + \frac{t_4 - t_3}{2} \right) \\ + \frac{2T - (t_4 - t_{\text{arc}}^{\min})}{2T} * \left(t_{\text{arc}}^{\min} + \frac{t_5 - t_4}{2} \right) \\ = t_{\text{arc}}^{\min} + \frac{1}{4T} \left[(t_1 - t_{\text{arc}}^{\min})^2 + (t_2 - t_1)^2 \right. \\ \left. + (t_3 - t_2)^2 + (t_4 - t_3)^2 \right. \\ \left. + (2T - (t_4 - t_{\text{arc}}^{\min})) * (t_5 - t_4) \right] = 10.01 \text{ ms.} \quad (17)$$

The exact average arcing time need to randomize all the influential parameters listed in Table II from practical data [25]. Due to space limitation, the detailed calculations on randomization of all the influential parameters are omitted here. After the randomization, the average arcing time for traditional breakers will be increased to

$$\overline{t'_{\text{arc}}} = 13.8 \text{ ms.} \quad (18)$$

Accordingly, our phase selection reduces the average arcing time from (15) to (18). In summary

$$t_{\text{arc}}^{\min} = \frac{5}{13.8} \overline{t'_{\text{arc}}} = 0.362 \overline{t'_{\text{arc}}}. \quad (19)$$

Since our smart circuit breaker can estimate the optimal zero crossing time through the real time current data, we can control

TABLE IV
MECHANICAL WEAR WITH DIFFERENT CONTACT SPEED

D_c (mm)	GCB w/o IO		Intelligent Operation GCB		
	12	8	9	10	12
$v_{average}$ (m/s)	4.8	3.6	3.9	4.3	4.8
W_m	W_{m0}	$0.750W_{m0}$	$0.813W_{m0}$	$0.896W_{m0}$	W_{m0}

the actual average arcing time to the optimum arcing time 5 ms, which is 36.2% of a circuit breaker without intelligent operation. Thus, the contact electrical wear will be nearly one third of its original value during fault current breaking.

B. Influence of Contact Speed on Mechanical Wear

Contacts mechanical wear is determined by factors such as contact movement, contact material, contact structure, and contact speed. Our selected GCB has copper-chromium alloy as contact material, and its contact structure is tulip contacts with sliding movement. Its main factor for mechanical wear is the contact speed.

From the pressure-wear theory [26], the mechanical wear volume of contact material can be written as

$$V_{vol} = K F_f S_d \quad (20)$$

where F_f is friction between static and moving contacts, which is proportional to the normal pressure force of the contact system; S_d is sliding distance; and K is a constant.

From (20), for an elemental area dA , we can find the rate of contact material change with respect to time

$$dV_{vol} = l dA = K(p dA) S_d \quad (21)$$

$$dl/dt = K p (dS_d/dt) \quad (22)$$

$$W_m = dl/dt = K p v \quad (23)$$

where l is the wear depth, p is contact normal spring pressure; v is sliding velocity at the over-travel stage; K is the constant. The mechanical linear wear rate W_m at any point within a sliding interface is defined in (23), which is proportional to the contact sliding velocity.

Denote the contact mechanical wear as W_{m0} for an average contact speed of $v_0 = 4.8$ m/s for conventional GCB. When the smart GCB is required to break rated current, it will be able to choose an appropriate speed characteristic; Table IV shows that contact mechanical wear increases proportional to the moving contact speed.

However, during a fault current interrupting, the smart GCB still operates at its fastest speed 4.8 m/s, and the mechanical wear will be the same as normal GCB.

V. CASE STUDY TO SHOW OUR IOGCB APPROACH CAN ENHANCE LIFE CYCLE OF BREAKERS

A. Without Intelligent Operation

A case study is performed to show that conventional life cycle experiments together with collected field data (both data are consistent with our model and calculations based on one single high contact speed without phase controls) can be employed to estimate the benefits of our ICU approach. The Siemens Corp. 145 kV SF₆ high-voltage power circuit breaker [28] data is used for the study, in which the breaker has a life cycle N_1 , 3000 operations, for its rated current 3 kA; and its life cycle is only N_2 , 18 operations, for fault current $I_{scN} = 40$ kA. According to the field data collected in [27], the constant $K_{w1} = 12.745$, $\beta_1 = 3$ for rated current $I_1 = 3$ kA, and $K_{w2} = 3.249$, $\beta_2 = 1.7$ for fault current $I_2 = 40$ kA for (8). Since I_1 and I_2 are constant values during experiments, the integration of (8) is simplified into algebraic computation. The arcing time is also simplified into the average arcing times for the case study since we are evaluating life cycle analysis that involves numerous operations, in which the arc starting time instants are random. Accordingly, the average electrical wear value only depends on the average arc duration time. As a consequence, the average arc duration value \bar{t}_{arc1} is the dominant factor for estimating the average electrical wear value. Based on (8), we can obtain the average electrical wear for both rated current and faulted current interruptions

$$W_{e1} = \int_0^{t_{arc1}} K_w |i_1(t)/I_{scN}|^{\beta_1} dt \quad (24)$$

$$W_{e2} = \int_0^{t_{arc1}} K_w |i_2(t)/I_{scN}|^{\beta_2} dt. \quad (25)$$

Then both accumulated electrical wears can be calculated for the Siemens GCB

$$\begin{aligned} W_e^{rated} &= N_1 \times W_{e1} = 3000 \times 12.745 \times (3/40)^3 \times \bar{t}_{arc1} \\ &= 16.13 \times \bar{t}_{arc1} \end{aligned} \quad (26)$$

$$\begin{aligned} W_e^{fault} &= N_2 \times W_{e2} = 18 \times 3.249 \times (40/40)^{1.7} \times \bar{t}_{arc1} \\ &= 58.50 \times \bar{t}_{arc1}. \end{aligned} \quad (27)$$

In which, average electrical wears for one single operation of two different operating conditions are described as

$$W_{e1} = 12.745 \times (3/40)^3 \times \bar{t}_{arc1} = 0.005377 \times \bar{t}_{arc1} \quad (28)$$

$$W_{e2} = 3.249 \times (40/40)^{1.7} \times \bar{t}_{arc1} = 3.249 \times \bar{t}_{arc1}. \quad (29)$$

Since the accumulated electrical wear during fault operations is much larger than the wear of all rated operations, the electrical wear of 18 fault operations dominates the failure limit for breakers. Therefore, (27) can be assumed as the breaker failure limit for the following calculations. On the other hand, the mechanical wear of rated operations, 3000, dominates the failure of rated operations.

B. Increased Mechanical Life Cycle With Speed Control

When using IOGCB to break rated current with a much slower speed, say at a speed of 3.6 m/s, the mechanical wear during each operation will be 75% of the value at 4.8 m/s per Table IV. Thus, our intelligent control can afford more rated operations; and the estimated life cycle for rated operations is

$$N'_1 = (N_1 \times W_{m0}) / (75\% \times W_{m0}) = 4000. \quad (30)$$

C. Electrical Wear Analysis With Speed Control Only

Due to the lower contact speed, the longer average arcing time for rated current operations is expected as shown from the third row of Table I: at a speed of 3.6 m/s, the average arcing time will be increases 1.333 times; and the total electrical wear during rated current operations is increased to

$$\begin{aligned} W_e^{r1} &= N'_1 \times W_{e1}^1 \\ &= 4000 \times 12.745 \times (3/40)^3 \times 1.333 \bar{t}_{arc1} \\ &= 28.70 \times \bar{t}_{arc1} \end{aligned} \quad (31)$$

which is still under its electrical wear limit in (27). Accordingly, the increased 4000 rated operations will not cause the smart breaker to have an electrical failure even though it may have reached the end of its mechanical life cycle in average.

D. Electrical Wear Analysis With Phase Selection Also

Based on the phase control technology discussed earlier, the average arcing time for rated current operations can be halved to further decrease its electrical wear. From fourth row of Table I, the average arcing time will be reduced to 66.7%. The total estimated electrical wear during rated current operations is computed in (32), which certainly do not exceed the wear limit value in (27) as shown below

$$\begin{aligned} W_e^{r2} &= N'_1 \times W_{e1}^2 = 4000 \times 12.745 \times (3/40)^3 \times 0.667 \bar{t}_{arc1} \\ &= 14.35 \times \bar{t}_{arc1}. \end{aligned} \quad (32)$$

On the other hand, the average arcing time during faults will be 36.2% of its original value due to phase selection, as in (19)

$$\begin{aligned} W_e^{f1} &= N_2 \times W_{e2}^1 \\ &= 18 \times 3.249 \times (40/40)^{1.7} \times 0.362 \bar{t}_{arc1} \\ &= 21.20 \times \bar{t}_{arc1} \end{aligned} \quad (33)$$

$$\begin{aligned} N'_2 &= (N_2 \times W_{e2}) / W_{e2}^1 \\ &= (N_2 \times \bar{t}_{arc1}) / (0.362 \bar{t}_{arc1}) = 49. \end{aligned} \quad (34)$$

Accordingly, phase control technology increases the conventional GCB' short-circuit fault life cycle from 18 to 49.

E. Remaining Life Cycle Estimation

Our novel IOGCB will have smaller electrical wear during every single operation, each rated operation wear W'_{e1} and each fault operation wear W'_{e2} can be calculated as follows:

$$W'_{e1} = 12.745 \times (3/40)^3 \times 0.667 \bar{t}_{arc1} = 0.003585 \times \bar{t}_{arc1} \quad (35)$$

$$W'_{e2} = 3.249 \times (40/40)^{1.7} \times 0.362 \bar{t}_{arc1} = 1.178 \times \bar{t}_{arc1}. \quad (36)$$

Suppose our smart GCB statistics tally indicates it has already performed N_r rated current operations and N_f short-circuit fault current operations. Our wear analysis can be used to estimate the remaining operation numbers of that breaker. The remaining wear estimate is calculated by the initial total wear minus the consumed wear

$$W_{\text{remaining}} = W_{\text{total}} - (N_r \times W'_{e1} + N_f \times W'_{e2}). \quad (37)$$

Therefore, the remaining life of the IOGCB will afford extra N_{r1} rated operations or N_{f1} fault operations

$$N_{r1} = \begin{cases} W_{\text{remaining}} / W'_{e1} & (\text{if } W_{\text{remaining}} / W'_{e1} \leq N'_1 - N_r) \\ N'_1 - N_r & (\text{if } W_{\text{remaining}} / W'_{e1} > N'_1 - N_r) \end{cases} \quad (38)$$

$$N_{f1} = W_{\text{remaining}} / W'_{e2}. \quad (39)$$

For example, if $N_r = 0$, $N_f = 0$, then $N_{r1} = 4000$, $N_{f1} = 49$, which means a brand new smart breaker will be able to open rated current up to a predicted number of 4000 times, or open faulted current up to 49 times. The life cycle has improved substantially from its original 3000 rated operations and 18 fault operations when our intelligence module is not used. Another example, when tally statistics indicates that $N_r = 1000$, $N_f = 10$, from (38) and (39), $N_{r1} = 3000$, $N_{f1} = 36$, which means that our IOGCB will have about 3000 additional rated current interruptions or another 36 fault current interruptions. The information can be served as a reference point for needed routine or just-in-time maintenance.

VI. CONCLUSION

A novel intelligent operation concept is proposed in this paper. The intelligent control unit consists of two main modules, smart switching and adjusting modules; further expansions, such as monitoring modules, display, and communication modules, can be added to enrich the intelligent functions of the intelligent control unit.

Based on the conventional SF₆ puffer type circuit breaker model, its moving characteristic analysis has been derived. Our analysis indicates that we can control GCB's intelligent operations by adjusting the drain oil aperture size; and the opening velocity can be selected adaptively according to actual power system working conditions.

Based on the derived moving characteristics, both electrical and mechanical wears are analyzed in terms of contact speeds. It is shown mechanical wear decreases due to slower contact speed; thus life cycle is increased substantially for rated normal operations. Phase control technology is developed to further reduce the electrical wear to increase the life cycles of its fault current operations. Finally, we demonstrate how to use conventional experimental data and field data to estimate the remaining life cycles using tallied statistics from our IOGCB. Siemens breaker data is used in our case study; and our IOGCB smart control unit is able to extend its mechanical life cycle from 3000 to a predicted number of 4000 times without exceeding

its electrical endurance limit. We can also extend the life cycle for faulted operations from 18 to about 49 theoretically. Our theoretical analysis remains to be evaluated and possibly modified in practice by more field data to estimate more precisely in the future. In conclusion, applying intelligent operation will help extend the lifetime of circuit breakers; longer life cycles will reduce both the equipment and maintenance cost, encourage smart grid applications to increase energy efficiency to further reduce the environmental impacts.

VII. DISCUSSION

Some rated-current situations need to be carefully designed while applying our various-speed interruption approach, such as switching unloaded transformers, reactors, generators, or shunt capacitor banks. These special considerations need to be further investigated and incorporated into our ICU by modifying the control software to cover the situations as described above. For example, if the smart CB is required to interrupt capacitive current, although it does not violate the short-circuit fault current threshold, the option to select the fastest speed to open should be available because of the easy reigniting nature of capacitive current.

REFERENCES

- [1] K. W. Hedman, R. P. O'Neill, E. B. Fisher, and S. S. Oren, "Optimal transmission switching with contingency analysis," *IEEE Trans. Power Syst.*, vol. 24, no. 3, pp. 1577–1586, Aug. 2009.
- [2] J. G. Rolim and L. J. B. Machado, "A study of the use of corrective switching in transmission systems," *IEEE Trans. Power Syst.*, vol. 14, no. 1, pp. 336–341, Feb. 1999.
- [3] A. A. A. El-Ela and N. T. T. Weig, "Line switching reconfiguration corrective action for overloads in power systems," in *39th Int. Universities Power Eng. Conf. (UPEC 2004)*, pp. 992–998.
- [4] A. Nguni and T. Le, "Interruptible load and demand response: World-wide picture and the situation in Sweden," in *Proc. 38th North Amer. Power Symp. (NAPS)*, Sep. 2006, pp. 121–127.
- [5] C. W. Yu, S. Zhang, T. S. Chung, and K. P. Wong, "Modelling and evaluation of interruptible-load programmes in electricity markets," *IEE Proc. Gener., Transm., Distrib.*, vol. 152, no. 5, pp. 581–588, Sep. 2005.
- [6] S. Yanabu, E. Zaima, and T. Hasegawa, "Historical review of high voltage switchgear developments in the 20th century for power transmission and distribution system in Japan," *IEEE Trans. Power Del.*, vol. 21, no. 2, pp. 659–664, Apr. 2006.
- [7] M. Homma, M. Sakaki, E. Kaneko, and S. Yanabu, "History of vacuum circuit breakers and recent developments in Japan," *IEEE Trans. Dielectr. Electr. Insul.*, vol. 13, no. 1, pp. 85–92, Feb. 2006.
- [8] R. D. Garzon, *High Voltage Circuit Breakers: Design and Applications*, 2nd ed. Boca Raton, FL: CRC, 2002, pp. 170–171.
- [9] J. P. E. White, J. P. Dupraz, and G. F. Montillet, "Strategy for applying a digital SF₆ monitoring device to high voltage circuit breakers," in *Proc. 2003 IEEE Power Eng. Soc. Gen. Meet.*, pp. 2223–2227.
- [10] M. Kezunovic, Z. Ren, G. Latisko, D. R. Sevcik, J. S. Lucey, W. E. Cook, and E. A. Koch, "Automated monitoring and analysis of circuit breaker operation," *IEEE Trans. Power Del.*, vol. 20, no. 3, pp. 1910–1918, Jul. 2005.
- [11] *IEC Standard for High Voltage Switchgear and Controlgear—Part 100: High-Voltage Alternating-Current Circuit-Breakers*, IEC 62271-100, Oct. 2006.
- [12] P. L. Fletcher and W. Degen, "A summary of the final results and conclusions of the second international enquiry on the reliability of high voltage circuit-breakers," in *Proc. 2nd Int. Conf. Rel. Transm. Distrib. Equipment 1995*, pp. 24–30.
- [13] Phadke, G. Arun, Thorp, and S. James, *Computer Relaying for Power Systems*, 2nd ed. New York: Wiley, 2009.
- [14] LW35-72.5/126/145 Circuit Breakers [Online]. Available: [Online]. Available: <http://www.pinggao.com>

- [15] L. Xu, X. Chen, and Z. Ma, "Calculation of the dielectric recovery characteristics without load of SF₆ circuit breaker," *Proc. Chin. Soc. Electr. Eng.*, vol. 18, no. 5, pp. 315–318, Sep. 1998.
- [16] X. Chen, Z. Ma, and L. Xu, "Study on the opening moving characteristic of the puffer circuit breaker," *High Voltage Technol.*, vol. 24, no. 4, pp. 21–25, Dec. 1998.
- [17] W. Shi, *Hydraulic Mechanism of Breaker*. Beijing, China: Mech. Eng. Press, 1990, p. 81.
- [18] L. I. U. Xinghua and L. I. Guangrong, "Research and test of high speed switch electromagnetic valve," *Chin. Internal Combustion Engine Eng.*, vol. 25, no. 1, pp. 38–42, Mar. 2004.
- [19] X. Zhang, Z. Y. Ma, and G. Wang, "Mathematical simulation of breaking characteristics of an SF₆ puffer interrupter," in *Proc. 1993 2nd Int. Conf. Electr. Contacts, Arcs, App. Their Appl.*, Xi'an, China, pp. 79–82.
- [20] B. Zhang, "Designing and computing on oil buffer," *High Voltage App.*, no. 6, 1977.
- [21] H. Huang, "Design and implementation of controller for intelligent operation circuit breaker," M.S. thesis, Dept. Electr. Eng., Xi'an Jiaotong Univ., Xi'an, China, 2006.
- [22] M. G. Diehl, "Wear of electrical contacts," *Wear*, vol. 1, no. 5, pp. 367–376, 1958.
- [23] W. Hu, X. Yin, Z. Zhang, J. Wu, and D. Shao, "Electrical endurance simulation of high voltage circuit breaker contact based on matlab," *China Proc. Elect. Power Syst. Autom.*, vol. 15, no. 6, pp. 9–12, Dec. 2003.
- [24] B. J. Ware, "Synchronous switching of power systems," presented at the Int. Conf. Large High Voltage Elect. Syst., Session 13–205, Paris, France, Aug. 1990.
- [25] J. Liu and Z. Ma, "A novel algorithm for online real-time calculation of short-circuit current," in *Proc. 16th Int. Conf. Gas Discharge Their Appl.*, Sep. 2006, pp. 2745–2749.
- [26] P. Reichner, "Pressure-wear theory for sliding electrical contacts," *IEEE Trans. Compon., Hybrids, Manuf. Technol.*, vol. 4, no. 1, pp. 45–51, Mar. 1981.
- [27] A. Pons, A. Sabot, and G. Babusci, "Electrical endurance and reliability of circuit-breakers-common experience and practice of two utilities," *IEEE Trans. Power Del.*, vol. 8, no. 1, pp. 168–174, Jan. 1993.
- [28] SF₆ High voltage power circuit breakers, dead tank [Online]. Available: <http://w3.energy.siemens.com/cms/us>



power system reliability.

Jun Liu (S'09) received the B.S. degree in electrical engineering in 2004 from Xi'an Jiaotong University, Xi'an, China. He is currently working toward the Ph.D. degree at the State Key Laboratory of Electrical Insulation and Power Equipments, Department of Electrical Engineering, Xi'an Jiaotong University, and is a visiting Ph.D. student at Texas A&M University, College Station.

His interest is with intelligent controls of high-voltage circuit breakers, power equipment reliability, power system operation and control, and



Garg M. Huang (M'80–SM'85) received the B.S. and M.S. degrees in electrical engineering from National Chiao Tung University, Hsinchu, Taiwan, in 1975 and 1977, respectively, and the Ph.D. degree in system science and mathematics from Washington University, St. Louis, MO, in 1980.

He taught at Washington University from 1980 to 1984. He joined the Department of Electrical Engineering, Texas A&M University, College Station, in 1984. He is currently a Professor and the Director of Graduate Studies there. He has published more than

one hundred papers and reports in the areas of nonlinear, distributed control systems, parallel/distributed computing and their applications to power systems, data networks and flexible structures. He have been working on many funded research projects, such as emergency control of large interconnected power systems, HVDC systems, restoration of large scale power systems, online detection of system instabilities, and online stabilization of large power system, fast parallel/distributed textured algorithm for data network routing problem, etc.

Dr. Huang is a Registered Professional Engineer of Texas. He has served as the Technical Committee Chairman of Energy System Control Committee and an Associate Editor in the IEEE Automatic Control Society; he has also been serving in a number of committees and subcommittees of the IEEE PAS Society.



Zhiying Ma (M'82–SM'94) received the B.S. and M.S. degrees from the Department of Electrical Engineering of Xi'an Jiaotong University, Xi'an, China, in 1959 and 1963, respectively.

From August 1987 to September 1988, he was a Visiting Scholar at Strathclyde University, U.K. Since 1958, he has been teaching and researching at Division of Electrical Apparatus of Xi'an Jiaotong University. He was promoted to Professor in 1992. His research areas are theory of electric arc, high and low voltage switchgear, fuse, intelligent operation of

circuit breaker, theory and development of new type high-voltage switchgear.

Prof. Ma is a Member of the Committee on China High Voltage Switchgear Standardization, a Member of the China Electrotechnical Society (CES), Director of Electric Contact and Electric Arc Committee of CES, and Vice Director of Power Transmission and Transformation Committee of China Society of Electrical Engineering (CSEE).



Yingsan Geng (M'89–SM'99) received the B.S., M.S., and Ph.D. degrees in electrical engineering from Xi'an Jiaotong University, Xi'an, China, in 1984, 1987, and 1997, respectively.

He is currently the vice president of State Key Laboratory of Electrical Insulation and Power Equipments, Xi'an Jiaotong University. Since 1987, he has been teaching and researching in the Division of Electrical Apparatus of Xi'an Jiaotong University. He was promoted to Professor in 2001. His research interest focuses on theory and application of power

equipments, intelligent circuit breaker in smart grid, high-voltage vacuum circuit breakers development, and computer-aided design and simulation of electric apparatus.